# Electronic Supplementary Information (ESI)

## On-chip polyelectrolyte coating onto magnetic droplets – Towards continuous flow assembly of drug delivery capsules

Ali. Q. Alorabi,[a,‡] Mark D. Tarn,[a,§] Jenifer Gómez-Pastora,[a,b] Eugenio Bringas,[b] Inmaculada Ortiz,[b] Vesselin N. Paunov[a] and Nicole Pamme*[a]

[a.] *School of Mathematics and Physical Sciences, University of Hull, Cottingham Road, Hull, HU6 7RX, UK. E-mail: n.pamme@hull.ac.uk; Tel: +44 (0) 1482 465027; Fax: +44 (0) 1482 466410.*

[b.] *Department of Chemical and Biomolecular Engineering, University of Cantabria, Av. de los Castros s/n, 39005 Santander, Cantabria, Spain.*

‡ Current address: *Albaha University, Prince Mohammad Bin Saud, Al Bahah 65527, Saudi Arabia.*

§ Current address: *School of Earth and Environment, University of Leeds, Leeds, LS2 9JT, UK*.

**CONTENTS**



**VIDEOS**

**ESI Video 1 - Droplet deflection in shallow chip design.mp4**

**ESI Video 2 - Droplet generation in deep chip design DGF4.mp4**

**ESI Video 3 - Droplet deflection in deep chip design.mp4**

**ESI Video 4 - Droplet deflection in Snakes-and-Ladders chip design.mp4**

## 1. Droplet generation and deflection in shallow chip design

### *1.1 Chip designs*

Three shallow chip designs (DGF1, DGT2 and DGT3) were used for droplet generation (Fig. S1), each having a different type of droplet generation region that fed into an otherwise identical reaction chamber. All designs were etched into a single glass plate (1 mm thick) to a depth of 20 μm using conventional photolithography and wet etching techniques, then thermally bonded to a second, unetched glass plate (1 mm thick). Scale bars were also included in the design (not shown), above and below the reaction chamber, to assist in placement of the magnet. Design DGF1 (Fig. S1a) featured a flow-focusing junction with a 100 μm wide inlet (inlet 1) for the aqueous continuous phase (CP), and a 50 μm wide inlet (inlet 2) for the organic dispersed phase (DP). The droplet generation nozzle was 50 μm wide. Designs DGT2 (Fig. S1b) and DGT3 (Fig. S1c) each featured a T-junction for droplet generation, with two inlets (1 and 2) used for the organic DP; the DGT2 DP inlets had a width of 120 μm, while those of DGT3 had a width of 60 μm. The aqueous CP was introduced through inlet 3, positioned perpendicular to inlets 1 and 2; that of DGT2 was 120 μm wide, while the DGT3 channel was 60 μm wide. The reaction chamber was 8.04 mm long and 2.74 mm wide (after etching), and the multiple branched inlet and outlet channels leading into and out of the chamber, respectively, were each 120 μm wide.

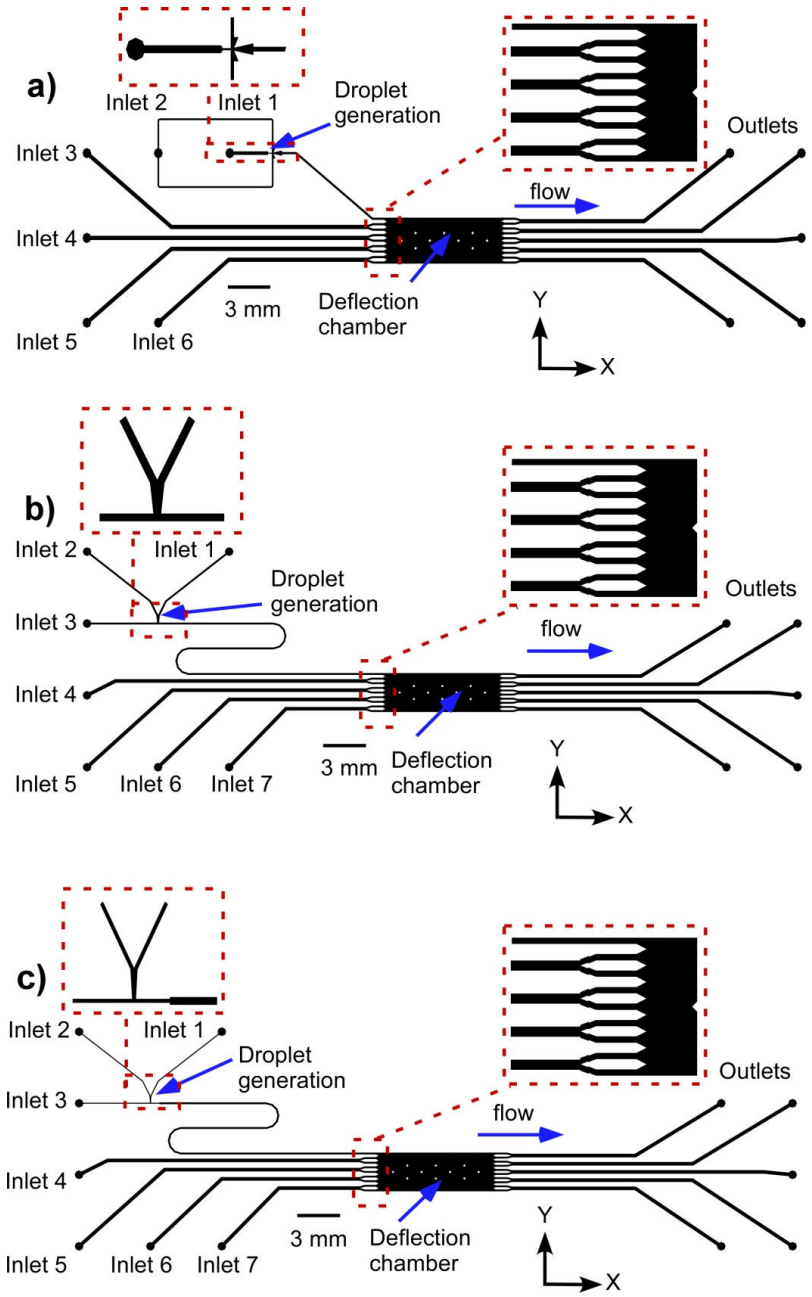


**Fig. S1** Shallow chip designs, each etched to a depth of 20 µm and having an identical reaction chamber (8.04 mm long by 2.74 mm wide after etching). (a) Design DGF1 for droplet generation via a flow-focusing junction (50 µm wide DP channel, 100 µm wide CP channel). (b) Design DGT2 featuring a T-junction with 120 µm wide channels. (c) Design DGT3 featuring a T-junction channel with 60 µm wide droplet generation channels. The designs also featured scale bars for magnet placement (not shown).

### *1.2 Droplet generation*

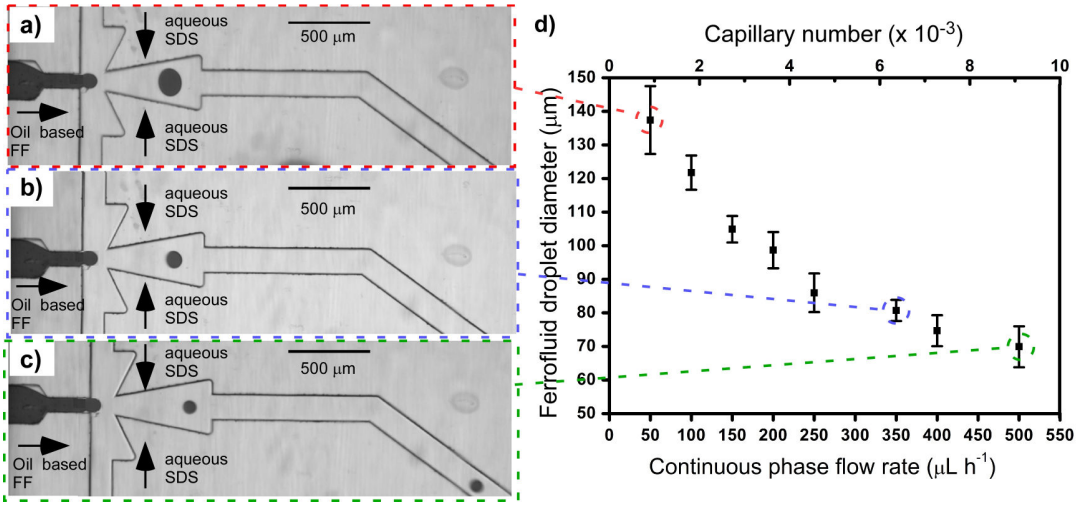


**Fig. S2** (a-c) Photographs of oil-based ferrofluid droplets generated in the shallow DGF1 chip design with increasing CP flow rate. The ferrofluid DP flow rate was 2 µL $h^{-1}$, while the aqueous CP (containing 1 % w/v sodium dodecyl sulfate, SDS) flow rate was varied from 50 to 500 µL $h^{-1}$. Droplets were disc-shaped in the microfluidic channels due to the 20 µm channel height. (d) Droplet size as a function of CP flow rate, demonstrating a decrease in droplet diameter with an increase in CP flow rate. The capillary number (*Ca*) is also shown as a function of the CP flow rate, which describes the ratio of the viscous forces to the interfacial forces: $Ca = \mu v/\gamma$, where $\mu$ and $v$ are the CP viscosity and velocity, respectively, and $\gamma$ is the interfacial tension between the fluids. Low capillary numbers (~$10^{-3}$) indicate that interfacial forces dominate and droplet-based flow was therefore generated. $\eta$ was 1.002 x $10^{-3}$ kg $m^{-1}$ $s^{-1}$, while $\gamma$ between the ferrofluid and aqueous SDS solution was determined to be 5 mN $m^{-1}$ via a tensiometer (TVT 2, Lauda, Germany).

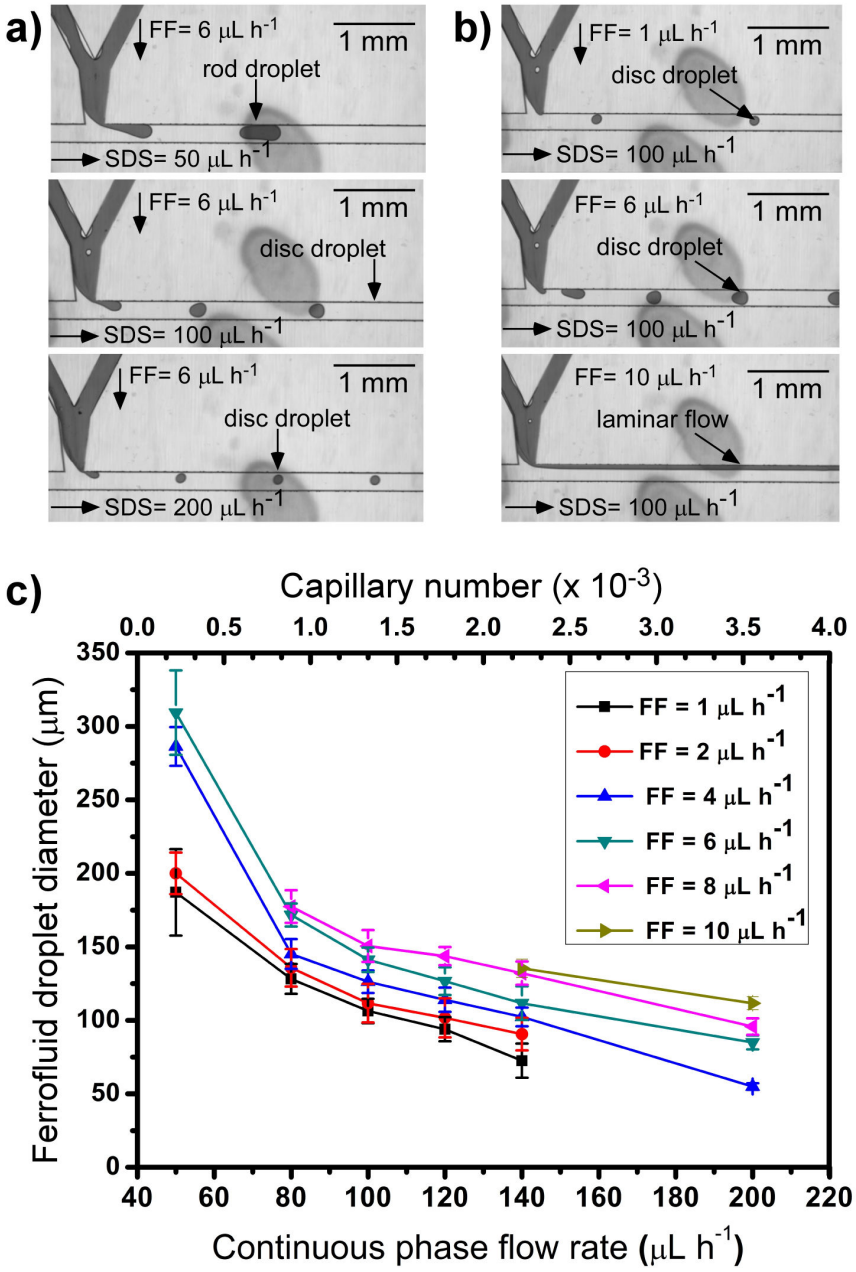


**Fig. S3** (a) Photographs of magnetic droplets generated in the shallow DGT2 chip design (20 μm depth) when the DP (ferrofluid) flow rate was fixed at 6 μL $h^{-1}$ and the CP (aqueous SDS) varied from 50 to 200 μL $h^{-1}$. Droplet diameters decreased with increasing CP flow rate. (b) Photographs of magnetic droplets generated in same chip design when the CP flow rate was held constant at 100 μL $h^{-1}$ and the DP flow rate was varied from 1 to 10 μL $h^{-1}$. Droplet sizes increased with increasing DP flow rate until laminar flow occurred. (c) Droplet diameter (n = 10 - 15) as a function of the CP and DP flow rates and capillary number, *Ca*.

### *1.3 Droplet deflection studies*

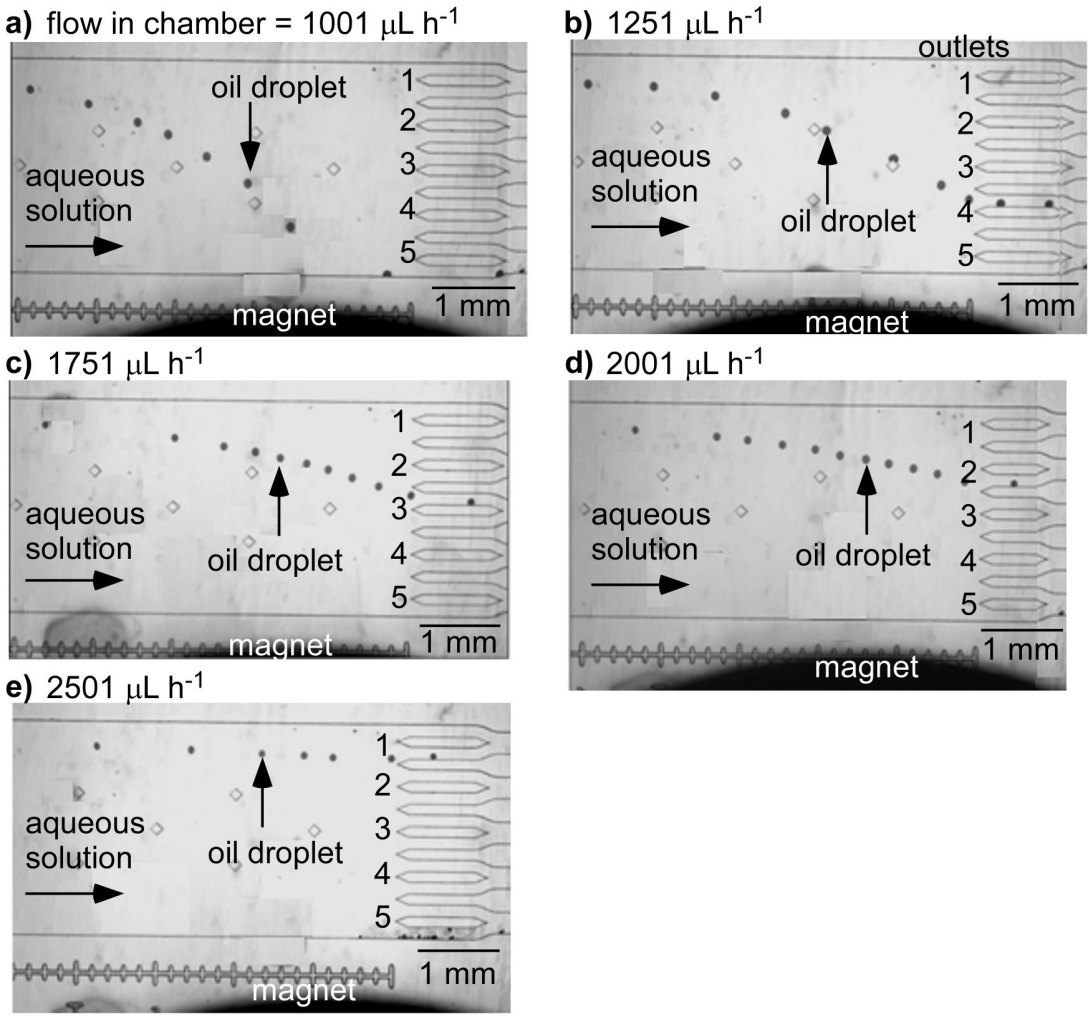


**Fig. S4** (a-e) Photographs of magnetic droplet manipulation in the reaction chamber (shallow chip design DGF1, 20 µm depth) via the use of a cylindrical 15 mm Ø x 5 mm NdFeB disc magnet. The droplets could be directed to each of the outlets (1 to 5) by varying the total flow rate in the chamber between (a) 1001 µL $h^{-1}$, (b) 1251 µL $h^{-1}$, (c) 1751 µL $h^{-1}$, (d) 2001 µL $h^{-1}$, and (e) 2501 µL $h^{-1}$.

**Table S1** The magnetic force ($\mathbf{F_{mag}}$) on the ferrofluid droplets in the chamber and their magnetically-induced velocity ($\mathbf{u_{mag}}$) in the y-direction at different flow rates. These results correspond to the experiments shown in Fig. S4. The outlet channel through which the droplets exited the chamber at each flow rate was also recorded.

| **Total flow rate in the chamber ($\mu L\ h^{-1}$)** | **Distance deflected in y-direction (mm)** | **Outlet through which droplets exited the chamber** | **Experimental $u_{mag}$ ($mm\ s^{-1}$)** | **Experimental $F_{mag}$ (nN)** |
|---|---|---|---|---|
| 1001 | 1.00 ± 0.08 | 5 | 2.5 ± 0.5 | 2.30 ± 0.48 |
| 1251 | 0.43 ± 0.02 | 4 | 1.4 ± 0.2 | 1.10 ± 0.16 |
| 1751 | 0.35 ± 0.07 | 3 | 1.3 ± 0.3 | 0.98 ± 0.23 |
| 2001 | 0.17 ± 0.13 | 2 | 1.2 ± 0.2 | 0.83 ± 0.22 |
| 2501 | 0.09 ± 0.02 | 1 | 0.5 ± 0.1 | 0.32 ± 0.07 |

### *1.4 Droplet deflection through a polyelectrolyte stream*

Once the feasibility of droplet deflection through streams of coloured inks had been verified (see Fig. 4 in the main manuscript), the next step was to test the deflection of droplets through a reagent stream of polyelectrolyte (PE) to enable coating of the droplets. Oil-based ferrofluid droplets were generated (DP = 1 μL $h^{-1}$ via inlet 1) in a continuous phase (CP = 100 μL $h^{-1}$ via inlet 2) of the solution of the anionic surfactant SDS, thereby yielding a negative charge upon the droplet surface. A laminar stream of aqueous solution of the cationic polyelectrolyte, poly(allylamine hydrochloride) functionalised with fluorescein isothiocyanate allylamine hydrochloride (PAH-FITC), was generated in the deflection chamber of the shallow DGF1 chip design via inlet 5 (see Fig. S1a), between streams of aqueous Tween20 (0.5 % v/v) solutions (through inlets 3, 4 and 6). The flow rates of the solutions pumped into inlets 3-6 was 200 μL $h^{-1}$ (total flow rate in the chamber = 901 μL $h^{-1}$, linear velocity = 4.58 mm $s^{-1}$). The droplets (100 ± 0.5 μm diameter) were able to flow freely through the aqueous Tween20 streams from inlets 3 and 4 whilst being deflected across the reaction chamber via a cylindrical 15 mm Ø x 5 mm NdFeB magnet. However, when the droplets reached the PAH-FITC interface, the ferrofluid would adhere to the chip surface, with the consequence that the magnetic droplets coalesced and spread throughout the region of the chamber that the PAH-FITC has interacted with (Fig. S5).

The main reason for this would likely be due to adsorption of the positively charged PAH-FITC polyelectrolyte onto the negatively charged glass surface, thus rendering the affected part of the channel surface positively charged. Therefore, as the negatively charged SDS-coated droplets crossed the chamber they would adhere electrostatically to the positively charged regions of the glass surface, which also facilitated their coalescence as the already adhered droplets encountered further droplets from upstream. This effect would be exacerbated by the fact that, in these shallow channels, the droplets would be flattened in the narrow space between the glass ceiling and floor of the chamber, thus forcing their interaction with the channel surfaces. This in turn leads to the undesirable binding of the droplets to the surface, followed by their coalescence and accumulation into larger droplets.

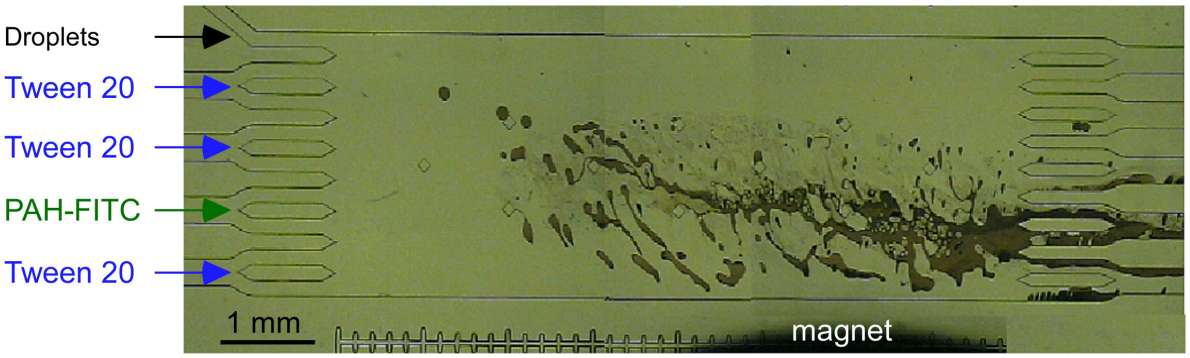


**Fig. S5** Photograph of magnetic droplets deflected through a stream of positively charged PAH-FITC via a cylindrical 15 mm Ø x 5 mm NdFeB disc magnet for the deposition of a layer of polyelectrolyte on the droplets in the shallow DGF1 chip. The PAH-FITC was found to yield a positive charge on the chip surface, resulting in adsorption and coalescence of the negatively charged magnetic droplets. Ferrofluid was pumped into inlet 1 at a flow rate of 1 µL $h^{-1}$, with aqueous SDS solution pumped into inlet 2 at a flow rate of 100 µL $h^{-1}$ for droplet generation. PAH-FITC was pumped into inlet 5, with Tween20 solution pumped into inlet 3, 4 and 6, each at a flow rate of 200 µL $h^{-1}$ (total flow rate in the chamber = 901 µL $h^{-1}$, linear velocity in chamber = 4.58 mm $s^{-1}$,magnetic force, $\mathbf{F_{mag}}$ = 0.6 nN).

## 2. Droplet generation and deflection in deep chip design

### *2.1 Chip designs*

Three chip designs were prepared for the fabrication of "deep" chips, featuring either a flow focusing (DGF4) or a T-junction (DGT5 and DGT6) droplet generation region. In each case, the droplet generation region was etched to a depth of 20 μm into the top plate (1 mm thick) of a glass device, while an interchangeable reaction chamber was etched to a depth of 100 μm into the glass bottom plate (1 mm thick) (Fig. S6). The reaction chamber featured an 8.2 mm long by 4.3 mm wide reaction chamber, with five inlet and five outlet channels (each 225 μm wide). One of the inlet channels consisted of a serpentine that lined up with the droplet generation region of each top plate design. The top plate of design DGF4 comprised a flow-focusing junction with a DP inlet channel of 50 μm width and a CP inlet channel of 100 μm width, with a droplet generation nozzle of 8 μm width (Fig. S6a). The top plate of design DGT5 featured a T-junction droplet generation region having CP and DP inlet channels of 8 μm width (Fig. S6b), while that of design DGT6 had a CP channel of 60 μm width and a DP channel that narrowed to 8 μm (Fig. S6c). The designs also featured a scale bar for magnet placement (not shown in the figures), located above and below the reaction chamber.

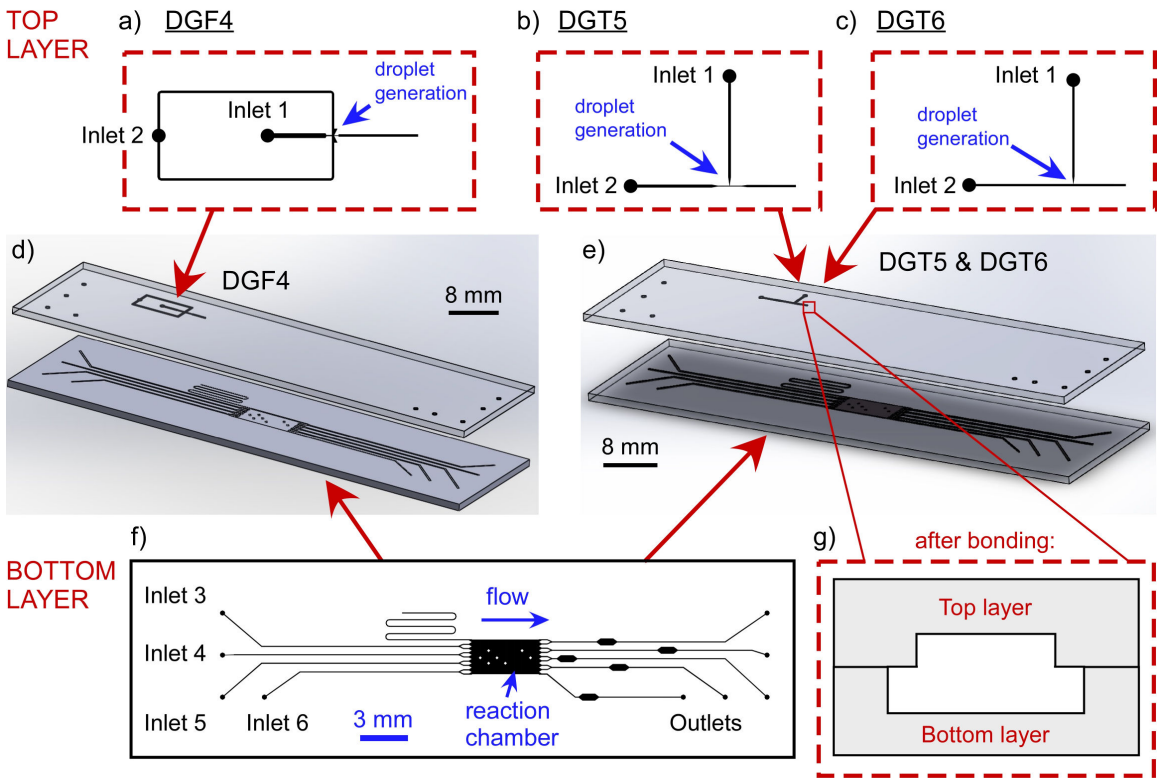


**Fig. S6** Deep chip designs, fabricated from two etched plates of glass, for the generation and deflection of droplets through polymer streams. In all cases, the droplet generation design was etched into the top plate to a depth of 20 µm and thermally bonded to an interchangeable bottom plate featuring an etched reaction chamber. Three types of top plate were fabricated: (a) Design DGF4 featured a flow focusing junction, comprising one inlet for the aqueous continuous phase (CP; 100 µm wide), one inlet for the organic dispersed phase (DP; 50 µm wide), and a nozzle (8 µm wide); (b) Design DGT5 featuring a T-junction with one inlet for the aqueous CP (8 µm wide) and one inlet for the organic DP (8 µm wide) chip design for droplet generation and deflection; (c) Design DGT6 featuring a T-junction with an aqueous inlet (60 µm wide) an organic DP inlet (8 µm wide). (d) Schematic showing the assembly of the DGF4 top plate with the interchangeable bottom plate design. (e) Assembly of the DGT5 or DGT6 top plates with the interchangeable bottom plate. (f) Bottom layer featuring a reaction chamber (8.2 mm long and 4.3 mm wide) and the remaining inlet and outlet channels (each 225 µm wide), etched into a glass layer to a depth of 100 µm. The same bottom layer design was used for each type of droplet generation design, and the designs also featured scale bars for magnet placement (not shown). (g) Schematic showing the cross section of the thermally bonded channels where the droplet generation channel (top layer) feeds into an inlet channel of the reaction chamber (bottom layer).

### *2.2 Droplet generation studies*

Studies were carried out to establish the range of droplet sizes that could be produced with the three chip designs: a flow focusing design (DGF4), a narrow T-junction design (DGT5), and a wider T-junction design (DGT6). In each case, the flow rate of the ferrofluid in inlet 1 was kept constant at 1 µL $h^{-1}$ while CP of aqueous PVP solution (10 mg $mL^{-1)}$ was pumped into inlet 2 at flow rates between 50 and 500 µL $h^{-1}$. In each case, droplets were generated in the shallow part (20 µm depth) of the chip, adopting a flattened disc shape. When they entered the 100 µm deep channel, however, they had sufficient space to adopt a spherical shape (Fig. S7). Highly monodisperse droplets were generated, with diameters ranging from 35 to 90 µm (± 1.5 µm), as shown in Fig. 5b. The generation of droplets can be seen in "**ESI Video 2 - Droplet generation in deep chip design DGF4.mp4**". The size of the droplets was influenced by the dimensions of the channels as well as the flow rates. Faster flow rates of CP decreased droplet size in all three chip designs, as expected from previous observations. The smallest droplets were generated with the DGT5 design, which featured a narrow T-junction channel for the CP. For example, in the DGT5 chip, droplet diameters were 45.0 ± 0.9 µm at a CP flow rate of 100 µL $h^{-1}$, whilst in chip design DGT6 with a wider T-junction the droplets were 82.4 ± 1.5 µm in diameter at the same flow rate.

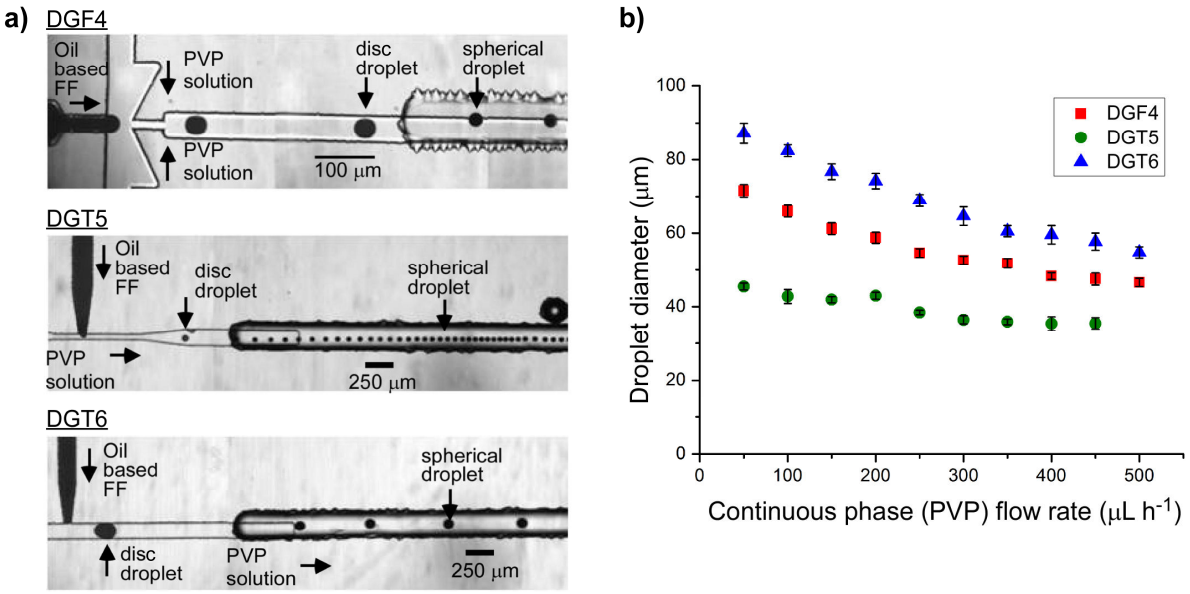


**Fig. S7** Generation of magnetic droplets in the "deep channel" chip design via three different droplet generation junctions. Droplets were formed from a dispersed phase of ferrofluid and a continuous phase of poly(vinylpyrrolidone) (PVP), forming a flattened disc-like shape in the 20 μm deep top layer, then being transferred into the 100 μm deep bottom layer where they adopted a spherical shape. (a) Droplet generation in the flow-focusing junction (DGF4), narrow T-junction (DGT5), and the wide T-junction (DGT6). (b) Magnetic droplet diameters as a function of PVP flow rate in each junction design. The ferrofluid flow rate was kept constant at 1 μL $h^{-1}$.

### *2.3 Droplet deflection studies*

The effect of magnetic flux density on the deflection of the magnetic droplets across the reaction chamber was investigated by varying the size of the rectangular NdFeB magnet used and its distance from the edge of the chamber in the deep DGF4 (flow-focusing) chip.

In the first instance, the effect of distance was studied using a 3 mm x 3 mm x 5 mm NdFeB magnet. The DP consisted of oil-based ferrofluid and was pumped into inlet 1 at a flow rate of 2 μL $h^{-1}$, while the CP contained an aqueous solution of poly(vinylpyrrolidone) (PVP, 10 mg $mL^{-1}$) that was pumped into inlet 2 at a flow rate of 500 μL $h^{-1}$, producing 47 ± 18 μm diameter droplets. PVP solution was pumped into the chamber via inlets 3−6 at a rate of 1000 μL $h^{-1}$ each, yielding a total flow rate in the chamber of 4502 μL $h^{-1}$ (linear velocity = 2.94 mm $s^{-1}$). Fig. S8 illustrates the different distances studied, alongside photographs of the resultant droplet deflection and a simulation of the magnetic flux density across the chamber generated using Finite Element Method Magnetics software (FEMM 4.2, available from www.femm.info). The magnet was positioned at distances of 1.5 mm (Fig. S8a), 2.5 mm (Fig. S8b) and 3.5 mm (Fig. S8c) from the lower edge (in the y-direction) of the chamber, significantly reducing the magnetic flux density (**B**) and its gradient ($\nabla$**B**) acting over the chip as the distance increased (Fig. S8d). Placement of the magnet was facilitated by the scale bars fabricated into the chip.

At a magnet distance of 1.5 mm from the edge of the chamber, the droplets traversed the entire width of the chamber and accumulated at its lower edge, with many being trapped there. At a magnet distance of 2.5 mm, the droplets also moved across the entire width of the chamber but, with lower magnetic velocities and forces, were able to exit via outlet 5. At a magnet distance of 3.5 mm, the droplets were found to only exit the chamber via outlet 3 due to the lower magnetic forces present.

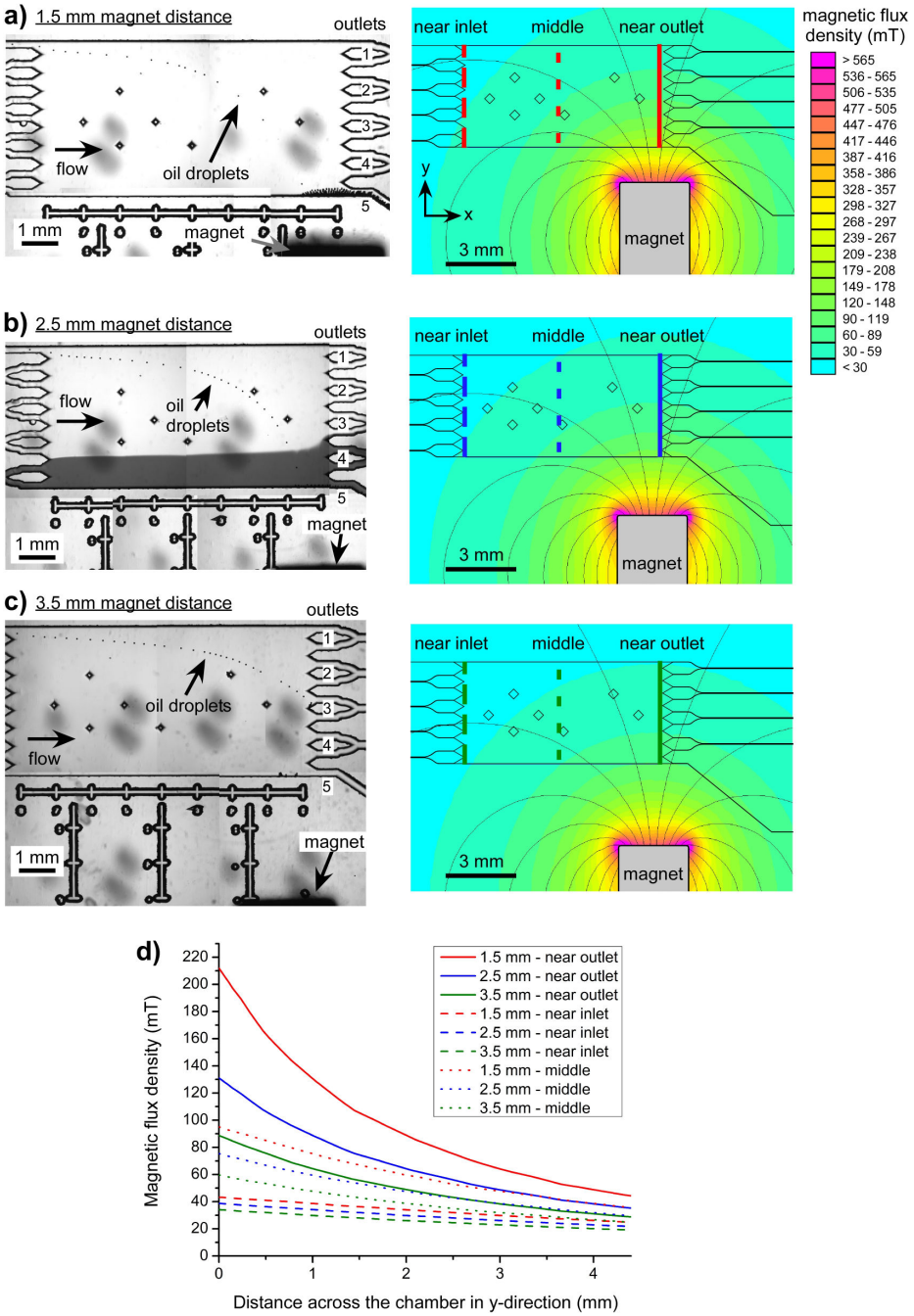


**Fig. S8** Photographs of droplet deflection and the corresponding magnetic simulations (FEMM 4.2) in the presence of a 3 x 3 x 5 $mm^3$ NdFeB magnet placed at varying distances from the edge of the chamber: (a) 1.5 mm, (b) 2.5 mm, and (c) 3.5 mm. The total flow rate in the chamber was 4502 µL $h^{-1}$ (2.94 mm $s^{-1}$). (d) The magnetic flux density (**B**) across the width (y-direction) of the reaction chamber at different locations in the x-direction (near the inlets, across the middle of the chamber, near the outlets), obtained from the FEMM simulations.

The effects of varying the magnet size are shown in Fig. S9. Rectangular NdFeB magnets having dimensions of 2 mm x 2 mm x 5 mm (Fig. S9a) and 3 mm x 3 mm x 5 mm (Fig. S9b) were positioned a distance of 3.5 mm from the edge of the separation chamber. Simulations of the magnetic flux density generated by the magnets in relation to the microfluidic chamber were created using FEMM 4.2 software. The larger magnet generated a magnetic flux density (**B**) and gradient ($\nabla$**B**) in the deflection chamber of about a factor of 2 greater than that of the smaller magnet, as shown in Fig. S9c.

At the flow rates employed in these experiments (FF = 2 μL $h^{-1}$, PVP = 300 μL $h^{-1}$, flow in chamber = 600 μL $h^{-1}$ x 4 inlets, total flow in chamber = 2702 μL $h^{-1}$, linear flow velocity in chamber = 1.76 mm $s^{-1}$), the droplets had an average diameter of 49.6 ± 1.5 μm and were deflected towards outlet 2 when using the smaller magnet ($\mathbf{F_{mag}}$ = 0.07 ± 0.01 nN, $\mathbf{u_{mag}}$ = 0.16 ± 0.01 mm $s^{-1}$). As expected by the FEMM simulations due to the increased **B** and $\nabla$**B**, the larger magnet deflected the droplets to a far greater extent than the smaller magnet, to the extent that they crossed the entire width of the chamber before exiting via outlet 5 ($\mathbf{F_{mag}}$ = 0.51 ± 0.02 nN, $\mathbf{u_{mag}}$ = 1.10 ± 0.05 mm $s^{-1}$).

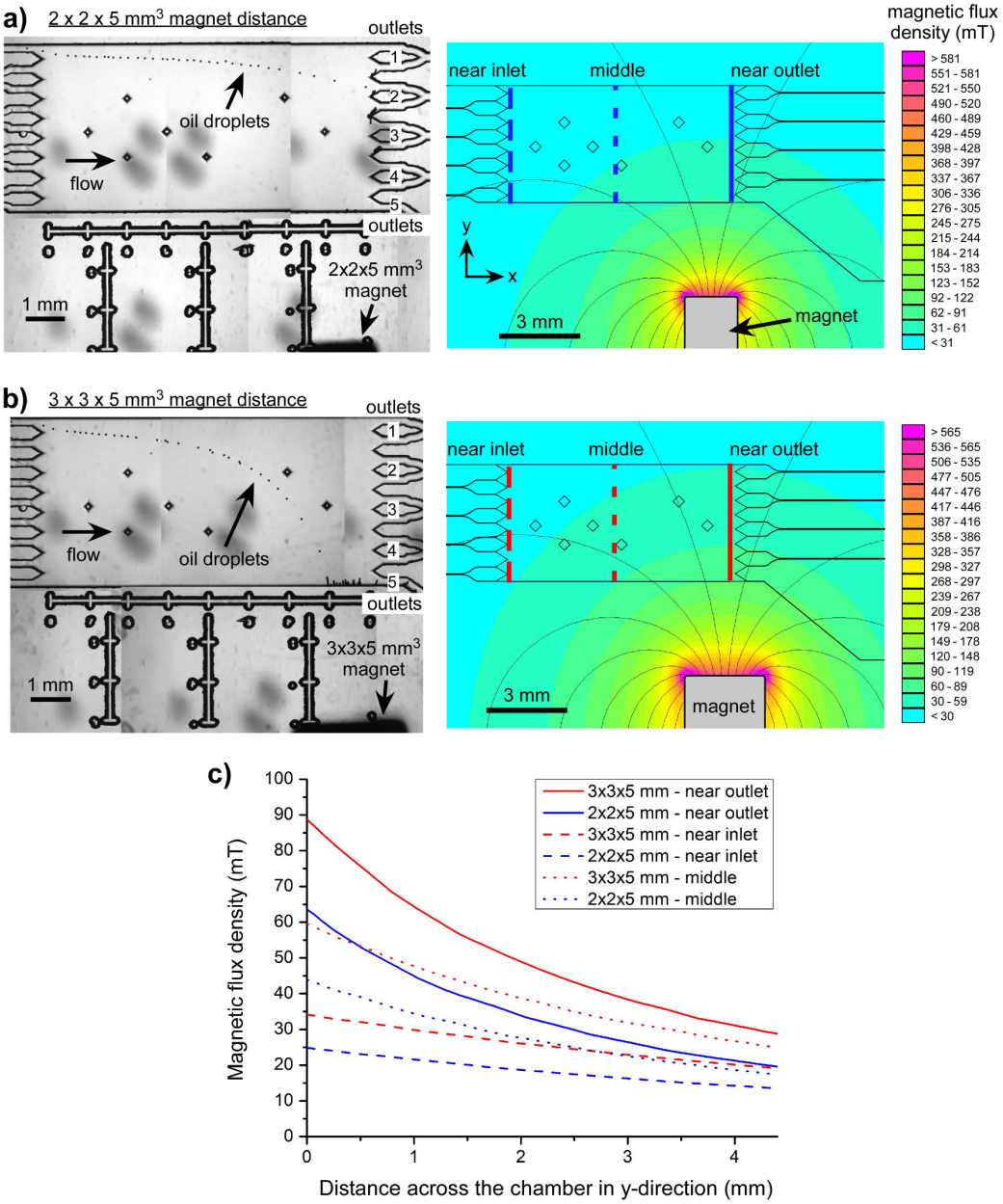


**Fig. S9** Photographs of droplet deflection and the corresponding magnetic simulations (FEMM 4.2) in the presence of rectangular NdFeB magnets with sizes of (a) 2 x 2 x 5 $mm^3$, and (b) 3 x 3 x 5 $mm^3$. The magnets were each placed 3.5 mm away from the lower edge (in the y-direction) of the reaction chamber, with their left-hand side lined up against a scale bar etched into the chip. The total flow rate in the chamber was 2702 µL $h^{-1}$ (1.76 mm $s^{-1}$). (c) The magnetic flux density (**B**) across the width (y-direction) of the chamber at different locations in the x-direction (near the inlets, across the middle of the chamber, and near the outlets), obtained from the FEMM simulations.

### *2.4 Magnetic loading of droplets*

After studying the effect of magnet size and position on deflection, the influence of magnetic particle concentration on a droplet at different magnet positions was also investigated in the deep DGF4 (flow-focusing) chip.

The stock solution of oil-based ferrofluid had a stated magnetic nanoparticle concentration of 2.25 x $10^{14}$ particles $\mu L^{-1}$, equivalent to 2.25 x $10^{6}$ particles $pL^{-1}$. This was diluted with cyclohexane to concentrations of 67 %, 50 %, 40 %, 33.3 %, 16.6 %, 9.1 % and 6.25 % of the original stock suspension, yielding particle concentrations of 15.0, 11.1, 9.0, 7.5, 3.7, 2.0 and 1.4 x $10^{7}$ particles $pL^{-1}$ (Table S2), respectively. Droplets were generated by pumping ferrofluid into inlet 1 at a flow rate of 0.5 $\mu L\ h^{-1}$ and aqueous PVP solution into inlet 2 at 100 $\mu L\ h^{-1}$. PVP solution was pumped into the chamber at a rate of 300 $\mu L\ h^{-1}$ via inlets 3-6 (total flow rate in chamber = 1300.5 $\mu L\ h^{-1}$, linear flow velocity = 0.85 mm $s^{-1}$). The number of magnetic particles per droplet was calculated for each ferrofluid concentration based on the droplet diameters obtained in each experiment (Table S2).

The previous study of the effect of magnet size and position had shown that, when using powerful neodymium-iron-boron (NdFeB) magnets (Magnet Sales, UK), the parameters required for the magnetic droplets to exit via outlet 5 brought them very close to the other outlets due to their steep trajectories. Hence, a 3 x 4.8 x 7.3 $mm^3$ sintered samarium cobalt magnet (SmCo, Magnet Sales, UK) was employed in order to provide smoother droplet trajectories through the chamber. The distance between the magnet and the lower edge (in the y-direction) of the chamber was varied between 10.5 mm, 8.5 mm and 6.5 mm (in a similar fashion to that described in Section 2.2). Simulations generated in FEMM 4.2 software demonstrated that the magnetic flux density (**B**) and gradient ($\nabla$**B**) acting over the chamber were significantly reduced as the magnet-to-chamber distance increased (Fig. S10a). The deflection of the magnetic droplets through the reaction chamber was evaluated for each ferrofluid concentration and magnet-to-chamber distance in terms of their magnetically induced velocity, $\mathbf{u}_{mag}$ (Fig. S10b), the magnetic forces acting on the droplets, $\mathbf{F}_{mag}$ (Table S3), and the outlet channel by which the droplets exited the chamber (Table S3).

**Table S2** Magnetic particle concentrations calculated for diluted ferrofluid, together with the average droplet diameters and volumes generated during experiments, and the estimated number of magnetic particles per droplet in each experiment.

| **Ferrofluid concentration (% of stock suspension)** | **Magnetic particle concentration (x $10^6$ particles $pL^{-1}$)** | **Average droplet diameter (μm)** | **Average droplet volume (pL)** | **No. of magnetic particles per droplet (x $10^9$)** |
|---|---|---|---|---|
| 100.0 | 2.25 | 66.7 | 155.4 | 34.96 ± 0.0002 |
| 67.0 | 1.50 | 54.1 | 82.9 | 12.44 ± 0.0007 |
| 50.0 | 1.12 | 52.4 | 75.3 | 8.45 ± 0.001 |
| 40.0 | 0.90 | 48.3 | 59.0 | 5.31 ± 0.00005 |
| 33.0 | 0.75 | 71.2 | 187.4 | 14.17 ± 0.0003 |
| 16.0 | 0.37 | 77.9 | 247.5 | 9.15 ± 0.00007 |
| 9.1 | 0.20 | 56.7 | 95.4 | 1.91 ±0.00001 |
| 6.3 | 0.14 | 58.1 | 102.7 | 1.44 ± 0.00003 |

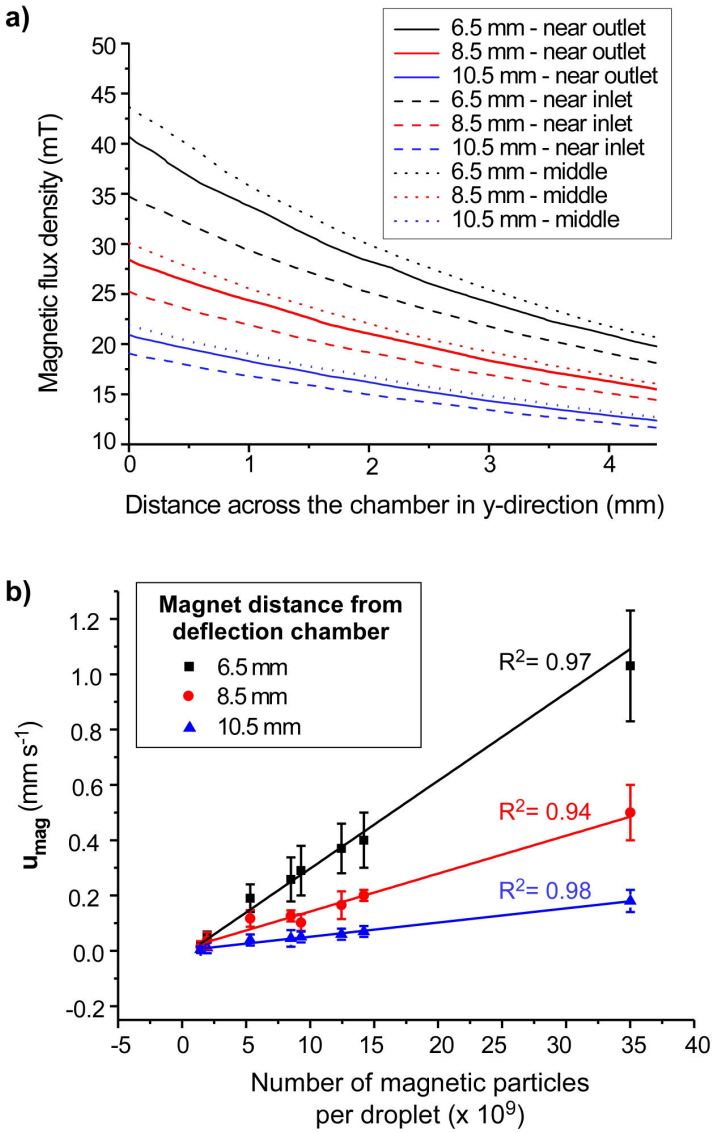


**Fig. S10** (a) Magnetic flux density (**B**) generated by a sintered samarium cobalt magnet (3 x 4.8 x 7.3 $mm^3$) across the width (y-direction) of the chamber of the deep DGF4 chip at different locations in the x-direction (near the inlets, across the middle of the chamber, and near the outlets). The magnet was placed at distances of 6.5 mm, 8.5 mm, and 10.5 mm from the lower edge (in the y-direction) of the chamber. See Fig. S7 for reference to how the magnet was positioned. (b) The magnetically induced velocity, $\mathbf{u}_{mag,}$ of the droplets across the reaction chamber as a function of the number of magnetic particles per droplet. The effect of the magnet-to-chamber distance on $\mathbf{u}_{mag}$ is also shown.

**Table S3** The magnetic forces ($F_{mag}$) on the ferrofluid droplets depending on their magnetic particle content and on the distance of the sintered samarium cobalt magnet from the edge of the reaction chamber. The outlet channel number by which the droplets exited the chamber are also given.

| **No. of magnetic particles per droplet (x $10^9$)** | **Distance between magnet and reaction chamber** | | | | | |
|---|---|---|---|---|---|---|
| | **10. 5 mm** | | **8. 5 mm** | | **6.5 mm** | |
| | **$F_{mag}$ (pN)** | **Outlet channel** | **$F_{mag}$ (pN)** | **Outlet channel** | **$F_{mag}$ (pN)** | **Outlet channel** |
| **34.96** | 107.08 | 5 | 314.94 | 5 | 642.48 | 5 |
| **12.44** | 106.70 | 5 | 134.47 | 5 | 366.07 | 5 |
| **8.45** | 32.39 | 4 | 84.29 | 5 | 153.27 | 5 |
| **5.31** | 32.36 | 4 | 75.01 | 5 | 213.28 | 5 |
| **14.17** | 31.68 | 3 | 62.38 | 5 | 127.74 | 5 |
| **9.15** | 29.19 | 3 | 72.53 | 5 | 110.12 | 5 |
| **1.91** | 6.21 | 1 | 19.81 | 5 | 26.77 | 5 |
| **1.44** | 2.74 | 1 | 8.23 | 2 | 6.58 | 3 |

### *2.5 Droplet deflection through ink streams*

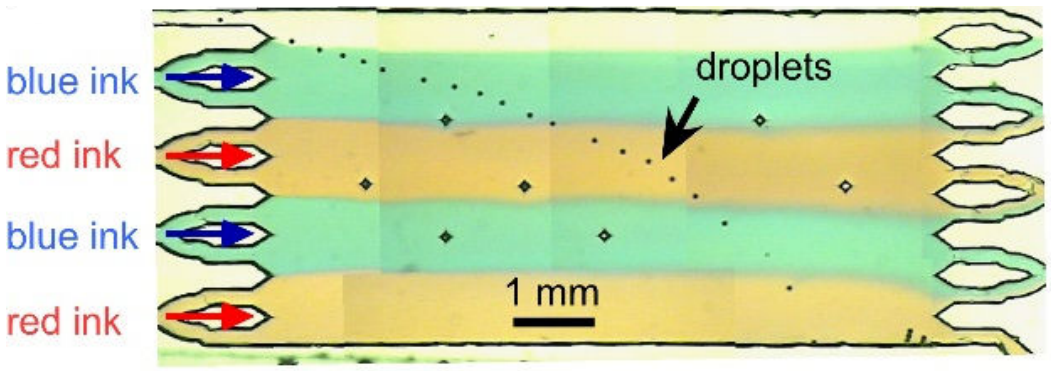


**Fig. S11** Photograph of ferrofluid droplets deflected through multilaminar streams of alternating red and blue inks using a sintered samarium cobalt magnet (7.3 mm x 4.8 mm x 3 mm) in the deep DGF4 chip. The magnet was placed 7.5 mm from the lower edge (in the y-direction) Ferrofluid (diluted 1:1 with cyclohexane; 1.12 x $10^6$ particles $pL^{-1}$) was pumped into inlet 1 at a flow rate of 1 µL $h^{-1}$, with aqueous SDS solution pumped into inlet 2 at 100 µL $h^{-1}$ for the generation of droplets. The red and blue aqueous inks were pumped into inlets 3-6 at a rate of 200 µL $h^{-1}$ each (total flow rate in chamber = 901 µL $h^{-1}$, linear velocity = 0.59 mm $s^{-1}$, $\mathbf{F_{mag}}$ = 0.1 nN). A video of droplet deflection through ink streams (taken via a black and white CCD camera) can be seen in "**ESI Video 3 - Droplet deflection in deep chip design.mp4**".

## 3. Droplet generation and deflection in “Snakes-and-Ladders” chip design

### *3.1 Droplet deflection through ink streams*

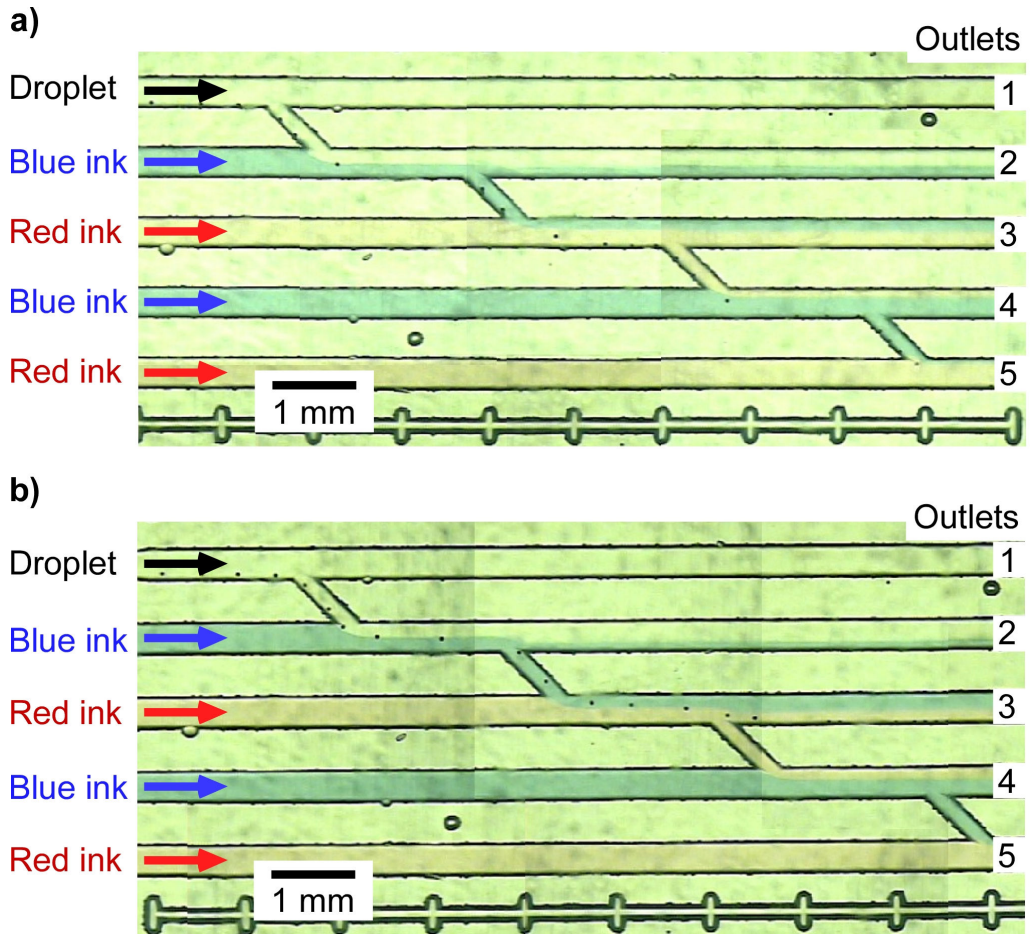


**Fig. S12** Effect of flow rate on droplet deflection through alternating blue and red ink streams across the “Snakes-and-Ladders” chip, using a sintered samarium cobalt magnet (7.3 mm x 4.8 mm x 3 mm) positioned 7.5 mm from the lower edge (in the y-direction) of channel 5. The ferrofluid dispersed phase flow rate in inlet 1 was 1 µL $h^{-1}$, while the PVP flow rate in inlet 2 was 300 µL $h^{-1}$. (a) When the inks were pumped into the chip at a flow rate of 300 µL $h^{-1}$ (2.08 mm $s^{-1}$) each, the droplets migrated through each channel and exited via outlet 5, thus passing through each ink stream. (b) When the flow rate of the inks was increased to 500 µL $h^{-1}$ (3.47 mm $s^{-1}$) each, the droplets were unable to pass through all of the ink streams and exited via outlet 3. A video of droplet deflection through ink streams can be seen in “**ESI Video 4 - Droplet deflection in Snakes-and-Ladders chip design.mp4**”.

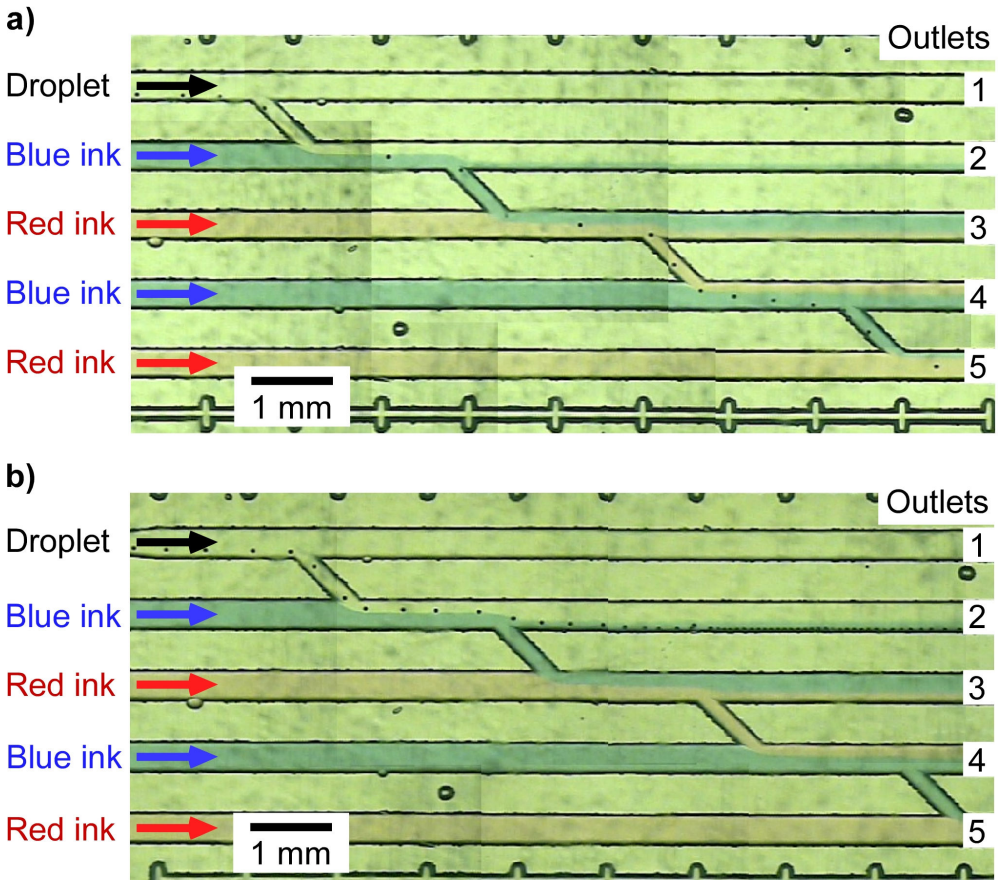


**Fig. S13** Effect of magnet position on droplet deflection through alternating ink streams across the "Snakes-and-Ladders" chip using a sintered samarium cobalt magnet (7.3 mm x 4.8 mm x 3 mm). The ferrofluid dispersed phase flow rate in inlet 1 was 1 μL $h^{-1}$, while the PVP flow rate in inlet 2 was 300 μL $h^{-1}$. (a) When the magnet was positioned 7.5 mm from the lower edge (in the y-direction) of channel 5, the droplets were able to cross each channel and thus be exposed to every ink stream. (b) When the magnet was positioned 10.5 mm from the lower edge of channel 5, the droplets only migrated as far as channel 2. The flow rate in each channel was 300 μL $h^{-1}$ (linear flow velocity = 2.08 mm $s^{-1}$ per channel).